

RADIO OBSERVATIONS REVEAL UNUSUAL CIRCUMSTELLAR ENVIRONMENTS FOR SOME TYPE IBC SUPERNOVA PROGENITORS

SARAH WELLONS¹, ALICIA M. SODERBERG¹, AND ROGER A. CHEVALIER²*Draft version March 14, 2019*

ABSTRACT

We present extensive radio observations of the nearby Type Ibc supernovae (SNe Ibc) 2004cc, 2004dk, and 2004gq spanning $\Delta t \approx 8 - 1900$ days after explosion. Using a dynamical model developed for synchrotron emission from a slightly decelerated shockwave, we estimate the velocity and energy of the fastest ejecta and the density profile of the circumstellar medium. The shockwaves of all three supernovae are characterized by non-relativistic velocities of $\bar{v} \approx (0.1 - 25)c$ and associated energies of $E \approx (2 - 10) \times 10^{47}$ erg, in line with the expectations for a typical homologous explosion. Smooth circumstellar density profiles are indicated by the early radio data and we estimate the progenitor mass loss rates to be $\dot{M} \approx (0.6 - 13) \times 10^{-5} M_{\odot} \text{ yr}^{-1}$ (wind velocity, $v_w = 10^3 \text{ km s}^{-1}$). These estimates approach the saturation limit ($\dot{M} \approx 10^{-4} M_{\odot} \text{ yr}^{-1}$) for line-driven winds from Wolf-Rayet stars, the favored progenitors of SNe Ibc including those associated with long-duration gamma-ray bursts. Intriguingly, at later epochs all three supernovae show evidence for abrupt radio variability that we attribute to large density modulations (factor of $\sim 3 - 6$) at circumstellar radii of $r \approx (1 - 50) \times 10^{16} \text{ cm}$. If due to variable mass loss, these modulations are associated with progenitor activity on a timescale of $\sim 10 - 100$ years before explosion. We consider these results in the context of variable mass loss mechanisms including wind clumping, metallicity-independent continuum-driven ejections, and binary-induced modulations. It may also be possible that the SN shockwaves are dynamically interacting with wind termination shocks, however, this requires the environment to be highly pressurized and/or the progenitor to be rapidly rotating prior to explosion. The proximity of the density modulations to the explosion sites may suggest a synchronization between unusual progenitor mass loss and the SN explosion, reminiscent of Type IIn supernovae. This study underscores the utility of radio observations for tracing the final evolutionary stage(s) of SN progenitor systems.

Subject headings: supernovae

1. INTRODUCTION

Type Ibc supernovae (SNe Ibc) are commonly understood to mark the death of massive stars, $M \gtrsim 10 M_{\odot}$. A relatively rare sub-group, SNe Ibc represent just 10-20% of all local SN discoveries (Cappellaro, Evans & Turatto 1999; Smartt 2009; Li *et al.* 2011). They are distinguished from other core-collapse SNe by the lack of hydrogen features in their optical spectra (see Filippenko 1997 for a review) indicating that their massive hydrogen envelopes are removed prior to explosion (Eliaset *al.* 1985; Filippenko & Sargent 1985; Wheeler & Levreault 1985; Uomoto & Kirshner 1985; Clocchiatti *et al.* 1986; Woosley, Heger & Weaver 2002). The lack of helium absorption features may further divide the sample into SNe Ic (helium-poor) and SNe Ib (He-rich; Matheson *et al.* 2001 but see Hamuy *et al.* 2002).

The physical mechanism and timescale on which SNe Ibc progenitors lose their envelopes, however, remains an open question. In a favored progenitor model, the metallicity-dependent (and often clumpy) line-driven wind of an isolated Wolf-Rayet (WR) star expels its own hydrogen envelope (Begelman & Sarazin 1986; Woosley, Langer & Weaver 1995). However, as argued by Smith & Owocki (2006), metallicity-independent continuum-driven winds and/or hydrodynamic eruptions may play a key role in the formation of Wolf-Rayet stars. A binary mechanism such as Roche lobe overflow, accretion or a common envelope phase could also remove the envelope of a massive progenitor (Wheeler & Lev-

reault 1985; Podsiadlowski, Joss & Hsu 1992; Yoon, Woosley & Langer 2010). Both single- and binary-star progenitors are similarly theorized for the $\sim 1\%$ of SNe Ibc associated with long-duration gamma-ray bursts (GRBs), characterized by a central engine-driven relativistic outflow (e.g., MacFadyen, Woosley & Heger 2001; Podsiadlowski, *et al.* 2004). However, the critical difference between ordinary SNe Ibc progenitors and those of GRB-SNe remains debated (e.g. Fryer *et al.* 2007).

Recent studies of the host galaxies of SNe Ibc and GRB-SNe have revealed surprising clues. Specifically, explosion site metallicity measurements suggest that GRB-SNe favor metal-poor environments more often than SNe Ic (Modjaz *et al.* 2008; Levesque *et al.* 2010). In parallel efforts, it has also been reported that SNe Ic reside in higher metallicity environs than SNe Ib (Anderson *et al.* 2010; Modjaz *et al.* 2011). These apparent environmental differences have been interpreted as evidence for a metallicity-dependent mass loss mechanism (e.g., Arcavi *et al.* 2010), such as line-driven winds (Castor, Abbott & Klein 1975; Conti 1978). However, direct observational constraints on the local (sub-parsec) circumstellar environments of the explosions are required to test this hypothesis.

The mass loss histories of single- and binary-star progenitors each produce unique density distributions in the circumstellar environment (e.g., smooth stellar wind profile, dense common envelope shell). The dynamical interaction between the ex-

¹Harvard-Smithsonian Center for Astrophysics, 60 Garden St., Cambridge, MA 02138, USA²University of Virginia, Astronomy Department, Charlottesville, VA 22904, USA

panding SN shockwave and the circumstellar medium (CSM) gives rise to non-thermal radio and X-ray emission that, in turn, traces the local mass distribution (Chevalier 1998). Radio and X-ray observations of young SNe Ibc are, in fact, the *only* way to reveal the mass loss histories of their progenitor stars in the final evolutionary stage. Motivated thus, the sample of SNe Ibc with detailed radio studies is growing, primarily as part of the Very Large Array Intensive Study of Naked Supernovae³ (ViSiONS; Berger, Kulkarni & Chevalier 2002; Berger *et al.* 2003a; Soderberg *et al.* 2005, 2006a,b,c; Soderberg 2007; Soderberg *et al.* 2008, 2010a,b).

The ViSiONS study has revealed several key findings to date, including (i) SNe Ibc radio luminosities span four orders of magnitude, $L_\nu \approx 10^{25} - 10^{29} \text{ erg s}^{-1} \text{ Hz}^{-1}$ (Soderberg 2007), and (ii) nearly half of all radio-detected SNe Ibc show evidence for small-scale (factor of ~ 2) light-curve modulations (e.g., SN 2003bg; Soderberg *et al.* 2006a). Both of these findings are attributed to a broad diversity in the mass loss histories of their progenitor stars (Chevalier & Fransson 2006). In parallel efforts, detailed radio studies of GRBs have revealed similar diversity in their circumstellar environments (e.g., Chevalier, Li & Fransson 2004), however, a direct comparison of the two samples has yet to be conducted.

Here we present extensive radio observations for three Type Ibc SNe – 2004cc, 2004dk, and 2004gq – all of which show large (factor of ~ 10) flux modulations at late epochs. Through our detailed modeling of the radio light-curves, we derive the properties of the shockwave (velocity, energy) and those of the circumstellar medium (density profile, progenitor mass loss rate). In all three SNe, we attribute the observed flux modulations to density modulations in the local environment. We compare the radio properties with those of other SNe Ibc and nearby central engine-driven explosions, including GRB-SNe 1998bw (Kulkarni *et al.* 1998) and 2006aj (Soderberg *et al.* 2006b) and the relativistic SN 2009bb (Soderberg *et al.* 2010a). In §2 we present the observations and in §3 we describe the dynamical model used to extract the properties of the shockwave and local environment and present the results of modeling the early radio data. In §4 we compare the models with the late-time radio data characterized by flux modulations. We discuss the implications of the observed flux variations in the context of circumstellar density modulations in §5 and, finally, in light of different channels for progenitor mass loss.

2. RADIO OBSERVATIONS

We observed SNe 2004cc, 2004dk, and 2004gq with the Very Large Array⁴ (VLA) shortly after optical discovery as part of the ViSiONS survey. In each case we detected a radio source coincident with the optical position and subsequently initiated an intense VLA follow-up campaign to study the temporal and spectral evolution of the radio emission. In Table 1 we summarize the basic properties of these SNe, including the spectroscopic classification, host galaxy distance estimate, and approximate explosion date. We adopt host galaxy distance estimates and integrated apparent magnitudes from NED⁵, including cosmology independent distances, when available.

³Here we use “naked” to describe supernovae from progenitor stars that have lost their hydrogen envelope prior to explosion.

⁴The Very Large Array is operated by the National Radio Astronomy Observatory, a facility of the National Science Foundation operated under cooperative agreement by Associated Universities, Inc.

⁵<http://nedwww.ipac.caltech.edu>

Radio data were collected at multiple frequencies between 1.43 and 43.3 GHz (Tables 2-4). The data were obtained in various array configurations as denoted in the Tables. All VLA observations were taken in the standard continuum observing mode with a bandwidth of $2 \times 50 \text{ MHz}$. At observing frequencies above 22 GHz, we included reference pointing scans to correct for the systematic 10-20 asec pointing errors of the VLA antennas. We used primary calibrators 3C48, 3C147, and 3C286 for flux calibration, while phase referencing was performed using a calibrator within 10 degrees. Data were reduced using standard packages within the Astronomical Image Processing System (AIPS). We fit a Gaussian model to the radio SN in each observation to measure the integrated flux density.

The radio light-curves for the three SNe are shown in Figures 1-5, spanning $\Delta t \approx 8 - 1900$ days after explosion, and are discussed in detail below. Their peak spectral luminosities span $L_\nu \approx (2 - 6) \times 10^{27} \text{ erg s}^{-1} \text{ Hz}^{-1}$, similar to other SNe Ibc and a factor of ~ 100 below the radio afterglow luminosities of nearby GRB-SNe and the engine-driven SN 2009bb. Intriguingly, all three SNe reveal evidence for large-scale (factor of ~ 10) light-curve variations at late time. We estimate the “abruptness” of the flux variations by determining the time interval between the epoch at which the modulation is first seen and the epoch of the previous observation (δt) and normalize by the time since explosion, Δt .

2.1. SN 2004cc

SN 2004cc was discovered on 2004 Jun 10.26 UT by the Lick Observatory Supernova Search (LOSS; Li *et al.* 2000) using the Katzmann Automatic Imaging Telescope (KAIT; Monard & Li 2004). The host galaxy, NGC 4568, is classified as SABC with an absolute B -band magnitude of $M_B \approx -19.6$ mag assuming a distance of $d \approx 18 \text{ Mpc}$. Spectral analysis revealed SN 2004cc to be a highly reddened SN Ic (Matheson *et al.* 2004; Foley *et al.* 2004). An unfiltered light-curve indicates a peak optical magnitude of $M \approx -16.2$ mag, less luminous than typical SNe Ibc (Li *et al.* 2011). However, this estimate does not account for host galaxy extinction which is likely to be significant (see Drout *et al.* 2011 for a discussion of extinction diagnostics for SNe Ibc).

Our first VLA observation was carried out on 2004 Jun 17 UT, roughly $\Delta t \approx 15$ days after explosion. We monitored the radio emission from SN 2004cc at frequencies, $\nu = 8.5, 15.0, 22.5$ and 43.4 GHz through $\Delta t \approx 1700$ days (Table 2 and Figure 2). At 8.5 GHz, the lightcurve reaches a peak of $F_\nu \approx 4.5 \text{ mJy}$ at $\Delta t \approx 28$ days with a spectral luminosity of $1.7 \times 10^{27} \text{ erg s}^{-1} \text{ Hz}^{-1}$. An abrupt steepening of the observed flux was observed at all frequencies at $\Delta t \approx 40$ days after explosion with a temporal profile at least as steep as $\Delta F_\nu \propto t^{-3.4}$ ($\nu = 8.46 \text{ GHz}$). Subsequently, the SN re-brightened at $\Delta t \approx 135$ days. We estimate the abruptness of these two episodes to be $(\delta t / \Delta t) \approx 0.27$ and $(\delta t / \Delta t) \lesssim 1.2$, respectively.

2.2. SN 2004dk

SN 2004dk was discovered by KAIT on 2004 Aug 1.19 UT (Graham & Li 2004). The host galaxy, NGC 6118 (morphology SAcD), has an absolute magnitude of $M_B \approx -19.4$ at $d \approx 23$

Mpc. Although SN 2004dk was originally classified as Type Ic, it was re-classified as a Type Ib following the detection of helium features (Filippenko *et al.* 2004). A late-time spectrum published by Maeda *et al.* (2008) reveals an ordinary hydrogen-poor SN Ib spectrum. Detailed optical photometry for SN 2004dk were reported by Drout *et al.* (2011) indicating a broad light-curve with a peak magnitude of $M_V \approx -18.2$ mag.

We first observed the SN with the VLA on 2004 Aug 7 UT, roughly $\Delta t \approx 8$ days after explosion. Table 3 summarizes our observations of SN 2004dk, taken at frequencies of $\nu = 4.9, 8.5, 15.0$ and 22.5 GHz. Comparable in spectral luminosity to SN 2004cc, it reaches a peak of $L_\nu = 1.6 \times 10^{27}$ erg s $^{-1}$ Hz $^{-1}$ at $\Delta t \approx 14$ days after explosion in the $\nu = 8.5$ GHz band. Similar to the case of SN 2004cc, radio monitoring revealed a re-brightening at $\Delta t \approx 4$ years after explosion (Stockdale *et al.* 2009) which was not evident in the previous observation at $\Delta t \approx 200$ days. We therefore estimate the abruptness of the modulation to be $\lesssim 7.7$.

We note that X-ray emission was also detected from SN 2004dk with XMM on 2004 Aug 12 UT ($\Delta t \approx 13$ days) with a flux, $F_X = 2.7 \pm 0.8 \times 10^{-14}$ erg cm $^{-2}$ s $^{-1}$ (0.5-8 keV; Pöoley 2007; Stockdale *et al.* 2009). At the distance of NGC 6118, this implies an X-ray luminosity of $L_X \approx 2 \times 10^{39}$ erg s $^{-1}$ and comparable to the X-ray luminosities of other ordinary SNe Ib observed on a similar timescale (e.g., SN 2008D; Soderberg *et al.* 2008). At this epoch, the spectral index (β ; $F_\nu \propto \nu^\beta$) observed between the radio and X-ray bands is $\beta_{RX} \approx -0.77 \pm 0.03$.

2.3. SN 2004gq

SN 2004gq was discovered independently by KAIT and the Stazione Astronomica di Sozzago Supernova Search on 2004 Dec 11.36 UT (Pugh *et al.* 2004). The host galaxy, NGC 1832 (morphology SBbc) and has an absolute B -band magnitude of $M_B \approx -20.1$ mag at a distance of $d \approx 26$ Mpc. SN 2004gq was also originally classified as Type Ic, but was later re-classified as Type Ib after the appearance of strong helium features in a spectrum obtained on 2005 Jan 7.3 UT (Modjaz & Falco 2005). As in the case of SN 2004dk, late-time spectroscopy by Maeda *et al.* (2008) indicated an ordinary hydrogen-poor SN Ib spectrum. Detailed optical photometry for SN 2004gq was presented by Drout *et al.* (2011) revealing a peak magnitude of $M_V \approx -17.6$ mag.

We initiated VLA observations of SN 2004gq on 2004 Dec 16 UT, roughly $\Delta t \approx 8$ days after explosion. Our observations of SN 2004gq are summarized in Table 4 spanning frequencies, $\nu = 1.4, 4.9, 8.5$ and 15 GHz. At 8.5 GHz, the SN reaches a peak luminosity of $L_\nu \approx 5.5 \times 10^{27}$ erg s $^{-1}$ Hz $^{-1}$ at $\Delta t \approx 21$ days. At $\Delta t \approx 400$ days, our observations reveal evidence for an abrupt *fading* at all frequencies. There are no subsequent radio observations available to determine if the emission later re-brightened. We estimate the abruptness factor of the radio steepening to be 0.21 and the power law decay to be at least as steep as $F_\nu \propto t^{-5.9}$.

3. A MODEL FOR THE RADIO EMISSION

Supernova observations are typically limited to the optical and near-IR bands where the signal is dominated by thermal emission from the inner, slow-moving layers of ejecta that carry the bulk of the kinetic energy. On the other hand, radio observations trace the outer, fastest-moving layer, the “shock-

wave”, to which only 0.01-0.1% of the total energy is coupled (e.g., Matzner & McKee 1999). Long duration GRBs are the notable exception, for which the relativistic jets and slower SN ejecta carry comparable energy, each approaching, and sometimes exceeding, $E \sim 10^{51}$ erg (e.g., GRB 030329; Berger *et al.* 2003b; Mazzali *et al.* 2003; Frail *et al.* 2005).

As the shockwave plows through the circumstellar medium, it shock-accelerates electrons into a power-law distribution of relativistic energies, $N(\gamma) \propto \gamma^{-p}$, above a minimum Lorentz factor, γ_m . The shockwave also generates amplified magnetic fields which cause the electrons to gyrate, emitting synchrotron radiation that peaks in the cm-band in the first days to weeks following the SN explosion. The synchrotron emission is suppressed at low frequencies due to absorption processes. In the case of SNe Ibc, Chevalier (1998) showed that the dominant absorption process is internal synchrotron self-absorption (SSA), whereas external absorption processes (e.g. free-free) may contribute significantly for some SNe II plowing into denser circumstellar environments with slower shock speeds (e.g., Fransson & Björnsson 1998). Self-absorption defines the spectral peak frequency for the synchrotron spectrum, ν_p , below which the radio spectral index is $\beta = 5/2$ (optically-thick) and above ν_p the spectral index is $\beta = -(p-1)/2$ (optically-thin; Rybicki & Lightman 1979). For SNe Ibc, a value of $p \approx 3$ is typical (Chevalier 1998). As the shockwave expands, the optical depth to SSA decreases, causing ν_p to cascade to lower frequencies with time.

3.1. Radio Spectral Energy Distributions

In our preliminary analysis of the SN data, we considered the multi-frequency radio observations from each epoch to examine the properties of the synchrotron spectrum at various stages in the radio light-curve evolution. As shown by Chevalier (1998), a radio SN spectral energy distribution is characterized by SSA is well described as, $F_\nu = 1.582 F_{\nu_p} (\nu / \nu_p)^{5/2} [1 - \exp(-(\nu / \nu_p)^{-(p+4)/2})]$. For each radio spectrum, we used a χ^2 minimization technique to determine p , ν_p , and the associated flux density at the spectral peak, $F_{\nu,p}$. The fitting routine was carried out independently at each epoch for which we obtained observations in at least three frequencies. The radio emission from all three SNe is well described by a SSA spectrum across multiple epochs (Figure 6). In each case, the electron energy index is consistent with $p \approx 3$ and the optically thick spectral index is not steeper than $\beta \approx 5/2$ indicating that any contribution from external absorption processes (e.g., free-free absorption) is negligible. As can be seen from the Figures, ν_p cascades to lower frequencies with time and is accompanied by a decrease in $F_{\nu,p}$.

We make the reasonable assumption that the post-shock energy density is equally fractioned between relativistic electrons (ϵ_e) and amplified magnetic fields (ϵ_B), i.e. equipartition, with the remaining energy coupled to shocked protons (ϵ_p). In this framework, the radius of the emitting material may be estimated from the spectral parameters measured at each epoch, $R \approx 5.7 \times 10^{15} (L_{\nu,p} / 10^{27} \text{ erg s}^{-1} \text{ Hz}^{-1})^{9/19} (\nu_p / 8.5 \text{ GHz})^{-1} \text{ cm}$. Here we have assumed that the emitting region occupies half of the total volume enclosed within a spherical shockwave. Combined with an estimate of the explosion date, the shockwave radius enables an estimate of the time-averaged shock velocity, \bar{v} .

Similarly, the strength of the amplified magnetic field may be estimated from the properties of the radio spectrum as $B \approx 0.93 (L_{\nu,p}/10^{27} \text{ erg s}^{-1} \text{ Hz}^{-1})^{-2/19} (\nu_p/8.5 \text{ GHz}) \text{ G}$. From this estimate, the total internal energy density of the radio emitting material is, $U \approx B^2/8\pi\epsilon_B$. It is reasonable to assume that the partition fractions are each constrained to be $(\epsilon_e, \epsilon_B) \lesssim 1/3$ (Chevalier 1998). A further constraint is implied by the shock velocity and the requirement that $\gamma_m \gtrsim 1$ leads to a lower limit on the electron partition fraction, $\epsilon_e \gtrsim 0.1(\bar{v}/0.2c)^{-2}$ for $p \approx 3$ (Soderberg *et al.* 2005; Chevalier & Fransson 2006; Soderberg *et al.* 2010b). In line with the typical velocities measured for SNe Ibc shockwaves, $\bar{v} \approx 0.2c$, we make the reasonable assumption that $\epsilon_e = \epsilon_B = 0.1$ throughout this paper.

3.2. A Dynamical Model

We adopt the formalism of Soderberg *et al.* (2005) in modeling the dynamics of the shockwaves. In this model, the shockwave parameters evolve self-similarly with time, $R \propto t^{\alpha_R}$ and $B \propto t^{\alpha_B}$. As shown by Chevalier (1982), the expansion of the slightly decelerated shockwave is characterized by $\alpha_R = (n-3)/(n-s)$ where n describes the density profile of the ejecta, $\rho_{\text{ej}} \propto r^{-n}$, and s describes the density profile of the circumstellar medium, $\rho_{\text{CSM}} \propto r^{-s}$. The self-similar model is constrained such that $n \geq 5$ and in the case of a stellar wind density profile, $s = 2$ and $\alpha_B = -1$. Using this general dynamical prescription, we fit the flux density measurements at each epoch and frequency simultaneously.

The flux density is parametrized as

$$F_\nu(t, \nu) = C_f \left(\frac{t}{t_0} \right)^{(4\alpha_R - \alpha_B)/2} [1 - e^{-\tau_\nu(t)}] \times \nu^{5/2} F_3(x) F_2^{-1}(x) \quad (1)$$

in $\text{erg/cm}^2/\text{s}/\text{Hz}$ where F_2 and F_3 are Bessel functions and $x \equiv 2/3(\nu/\nu_m)$ with ν_m defining the critical synchrotron frequency, $\nu_m \equiv 3\gamma_m^2 qB/(4\pi m_e c)$. The optical depth to SSA, τ_ν , evolves with time as

$$\tau_\nu(t, \nu) = C_\tau \left(\frac{t}{t_0} \right)^{(3+p/2)\alpha_B + (2p-3)\alpha_R - 2(p-2)} \times \nu^{-(p+4)/2} F_2(x) \quad (2)$$

where C_f and C_τ are normalization constants of the flux density and optical depth, respectively, and t_0 is a reference epoch. By fitting for C_f , C_τ , α_R , and α_B , we derived estimates for the physical parameters, R_0 , B_0 , and $\gamma_{m,0}$ at time, t_0 .

The number density of emitting electrons may be estimated from these parameters as, $n_e \approx B^2/(4\pi\gamma_m m_e c^2)$ where we maintain the assumption that $p \approx 3$ and $\epsilon_e = \epsilon_B$. Thus, the number density of shocked electrons scales temporally as $\alpha_{n_e} = 2\alpha_B - \alpha_\gamma$ and radially as $s = -(2\alpha_B - \alpha_\gamma)/\alpha_R$. The density of unshocked electrons in the circumstellar medium is related by the shock compression factor, η , such that $n_{\text{CSM}} = n_e/\eta$. The progenitor mass loss rate follows directly as $\dot{M} \approx 2\pi n_e m_p R^2 v_w$ where we have assumed a compression factor of $\eta = 4$ and a helium-rich stellar wind (nucleon-to-electron ratio of 2). Here, v_w is the velocity of the progenitor wind and we adopt $v_w = 10^3 \text{ km s}^{-1}$ as measured for Galactic Wolf-Rayet stars (Cappa, Goss & van der Hucht 2004; Crowther 2007). The temporal

evolution of the inferred mass loss rate is, $\dot{M} \propto t^{2\alpha_B+2}$, and is constant for a standard stellar wind profile with a steady wind velocity ($s = 2$).

3.3. Modeling Results

For each SN, we model the early radio data only, excluding the unusual late-time light-curve behavior in the fit. The temporal and spectral evolution of the SNe are well described by the dynamical model (Figures 2-5). For each SN, we report the two model parametrizations which best represent the data (see Table 5). In the primary fit, we used a χ^2 minimization technique to determine reasonable values for C_f , C_τ , α_R , and α_B . In the “standard” model fit, we fixed $s = 2$, $\alpha_B = -1$ and $\alpha_R = 0.9$ as expected in the typical scenario where the forward shock is only slightly decelerated (Chevalier & Fransson 2006), and fit only for C_f and C_τ . We extracted estimates for the physical parameters (R , B , E , and n_e) and their associated temporal and radial evolution. The results are detailed below for each SN and summarized in Table 5. We compare the temporal and radial evolution of the physical parameters for these three SNe in Figure 7.

In the case of SN 2004cc, the best fit is characterized by $\alpha_R \approx 0.9$, and a steep evolution of the magnetic field is required, $\alpha_B \approx -1.4$. Together these, imply a steep CSM density gradient, $s \approx 2.8$. At $t_0 = 10$ days, both models predict a velocity of $\bar{v}_0 \sim 0.1c$. However, the models differ regarding the energy, with the best fit model predicting an energy of $E_0 \approx 1.0 \times 10^{48}$ erg while for the standard model, $E_0 \approx 2.7 \times 10^{47}$ erg. Assuming the wind velocity is unchanged, the inferred mass loss rate varies with time; we estimate $\dot{M}_0 \approx 1.3 \times 10^{-4} \text{ M}_\odot \text{ yr}^{-1}$ at t_0 and just prior to the late-time re-brightening episode it is a factor of ~ 10 lower, $\dot{M} \approx 2.1 \times 10^{-5} \text{ M}_\odot \text{ yr}^{-1}$.

For SN 2004dk we find that the standard model provides an excellent description of the early radio data; our primary fit is not dissimilar from the standard model. We estimate a time-averaged shockwave velocity of $\bar{v}_0 \approx 0.2c$ and an energy of $E_0 \approx 1.7 \times 10^{47}$ erg at $t_0 = 10$ days. We find the progenitor mass loss rate to be constant, $\dot{M}_0 \approx 6.0 \times 10^{-6} \text{ M}_\odot \text{ yr}^{-1}$.

In the case of 2004gq, we find that the best fit is nearly consistent with a standard model, but with a shallower density profile, $s = 1.5$. In both models, the physical parameters at $t_0 = 10$ days are essentially the same. The implied time-averaged velocity is, $\bar{v}_0 \approx 0.25c$ and the energy is $E_0 \approx 5 \times 10^{47}$ erg. The implied progenitor mass loss rate is $\dot{M}_0 \approx 9 \times 10^{-6} \text{ M}_\odot \text{ yr}^{-1}$ and is not constant in the best fit model. Just prior to the epoch of the late-time flux steepening, the mass loss rate is $\dot{M} \approx 4 \times 10^{-5} \text{ M}_\odot \text{ yr}^{-1}$.

4. LATE-TIME FLUX VARIATIONS

Intriguingly, the late-time data for all three SNe reveal unusual behavior, in the form of a strong radio re-brightening for SNe 2004cc and 2004dk, and an abrupt fading for SN 2004gq. These late-time data were not included in the model fitting routines described above. For each SN, we measure the flux variation by comparing the late-time measurements (or limits) to an extrapolation of the model. In Table 5 we report the late-time flux modulation factor for each SN.

Radio variability in young SNe is typically caused by modulations in the circumstellar density profile, but engine-driven SNe may also produce radio variability due to off-axis ejecta components (jets) or prolonged central engine activity (see

Soderberg *et al.* 2006a for a discussion of radio SN variability). In the case of CSM density modulations, the flux variations are accompanied by a significant and abrupt shift in the location of synchrotron self-absorption frequency. This unique observational clue has enabled circumstellar density variations to be inferred for several core-collapse SNe exhibiting radio variability (Ryder *et al.* 2004; Soderberg *et al.* 2006a).

Chevalier (1998) show that for SNe dominated by SSA, $F_\nu \propto R^3 N_0 B^{(p+1)/2}$, where N_0 is the normalization of the electron energy distribution at $\gamma_m \approx 1$. Assuming ϵ_B is unchanged following an abrupt modulation in the circumstellar density, we have $B^2 \propto n_e v^2$ and thus expect roughly $F_\nu \propto n_e^{(p+5)/4}$ or $F_\nu \propto n_e^2$ for $p \approx 3$. Doubling the CSM density therefore produces a factor of ~ 4 increase in the optically-thin flux density. Assuming that the wind velocity is unchanged (a reasonable assumption since v_w is roughly set by the escape velocity) and the CSM density profile is characterized by $s = 2$, the implied mass loss rate modulation scales similarly, $\Delta F_\nu \propto \Delta \dot{M}^2$. In cases where $s \neq 2$, we adopt $\Delta F_\nu \propto \Delta \langle \dot{M} \rangle^2$ where $\langle \dot{M} \rangle$ represents a radially-averaged mass loss rate.

4.1. Mass Loss Variations

SN 2004cc shows evidence for a late-time re-brightening, nearly 100 times the flux density expected from an extrapolation of the model fits to the early data (Figure 2). The spectral index between frequencies of $\nu = 8.5$ and 15 GHz at $\Delta t \approx 130$ days is $\beta \approx -0.1$, indicating that the spectral peak was between these two frequencies at that time. However, ν_p cascaded through both frequencies several months earlier, indicating that the re-brightening is associated with an increase of ν_p . We therefore attribute the radio re-brightening to a significant circumstellar density modulation. A factor of ~ 11 increase in the optically-thin flux corresponds to a CSM density jump by a factor of ~ 3.3 and a mass loss rate of $\langle \dot{M} \rangle \approx 6.9 \times 10^{-5} M_\odot \text{ yr}^{-1}$.

More than four years after explosion, an abrupt re-brightening (factor of ~ 40) is observed for SN 2004dk and may be associated with a flattening of the spectral index between $\nu = 4.9$ and 8.5 GHz, $\beta \approx -0.2$ (Fig. 4)⁶. Similar to the case of SN 2004cc, the light-curves at these frequencies peaked much earlier and hence the re-brightening is associated with an upward shift of ν_p . We attribute this re-brightening to an increase in the circumstellar density by a factor of ~ 6 . A density modulation of this size implies an increased mass loss rate of $\langle \dot{M} \rangle \approx 3.5 \times 10^{-5} M_\odot \text{ yr}^{-1}$.

In the case of SN 2004gq, the late-time observations indicate a dramatic decline in the light-curves at $\Delta t \approx 400$ days. At this point, the flux density was below our detection threshold so a spectral index measurement was not possible, however, we note that the steepness of the decline ($F_\nu \propto t^{-6}$) is roughly consistent with the evolution expected for spherical adiabatic expansion losses of particles with an energy distribution of $p \approx 3$ and flux freezing (Shklovskii 1960; Kellermann & Pauliny-Toth 1968). Attributing the flux decline to a density drop, the measured upper limits imply a drop in the CSM density by a factor of $\gtrsim 5$. We constrain mass loss rate associated with this lower density wind to $\langle \dot{M} \rangle \lesssim 1.8 \times 10^{-5} M_\odot \text{ yr}^{-1}$.

In Figure 7, we compare the circumstellar density profiles for

⁶We note that the S/N of the late-time observations makes it difficult to precisely measure the spectral index. Further observations of SN 2004dk with the increased sensitivity of the EVLA are planned to follow the long-term evolution of the radio emission.

all three SNe as inferred from our dynamical modeling and including the abrupt modulations. Our radio observations point to significant (factor of $\sim 3-6$) circumstellar density modulations on radial scales of $r \approx (1-50) \times 10^{16} \text{ cm}$. Assuming a typical progenitor wind velocity of $v_w = 10^3 \text{ km s}^{-1}$, these density modulations are traced back to mass loss variations spanning a few years to a century prior to explosion.

4.2. A Comparison to Other Radio SNe

Our modeling of the early radio light-curves for SNe 2004cc, 2004dk, and 2004gq indicate mass loss rates spanning $\dot{M} \approx (0.6-13) \times 10^{-5} M_\odot \text{ yr}^{-1}$. However, these estimates vary by factors of $\sim 3-6$ following the observed late-time flux density modulations. In comparison with other radio SNe similarly observed on sub-parsec scales, these SNe represent examples of the strongest flux modulations ever reported. To date, such large-scale (factor of $\sim 5-10$) radio modulations have only been reported for a few SNe, including SN 1987A (Ball 1995; Zanardo *et al.* 2010), SN 1996cr (Bauer *et al.* 2008), SN 2001em (Stockdale *et al.* 2005), and SN 2007bg (Soderberg 2009).

Small-scale mass loss variations (factor of ~ 2) are more common and have been inferred for several core-collapse SNe including 1979C (Type IIL; Weiler *et al.* 1991), 2001ig (Type IIB; Ryder *et al.* 2004), 2003bg (broad-lined Type IIB; Soderberg *et al.* 2006a), and 2008ax (compact progenitor Type Ib/IIL; Roming *et al.* 2009; Chevalier & Soderberg 2010). Radio variability was also clearly seen for the relativistic central engine-powered 1998bw (associated with GRB 980425; Kulkarni *et al.* 1998) and 2009bb (Soderberg *et al.* 2010a; Bietenholz *et al.* 2010), both of which are broad-lined SNe Ic. However, it remains debated whether the variability was produced by central engine activity, additional ejecta components, or variations in the CSM density profile. Therefore, radio variability extends across the various SN Ibc sub-classes, including helium-rich, helium-poor, broad-lined, engine-driven and even hydrogen-rich (Type cIIL; Chevalier & Soderberg 2010). We stress, however, that density-induced flux variations are not ubiquitous as evidenced by several well-studied SNe with smooth radio light-curves including SN 1993J (IIL; (Weiler *et al.* 2007)), SN 2003L (Ic; Soderberg *et al.* 2005), SN 2008D (Ib; Soderberg *et al.* 2008), and GRB-SN 2003dh (i.e. the radio afterglow of GRB 030329; Berger *et al.* 2003b), each observed on similar sub-parsec radial scales.

We compare the radio-derived mass loss rates for SNe 2004cc, 2004dk, and 2004gq with those of other local SNe Ibc and engine-driven (GRB-SN) explosions within a comparable volume, $d \lesssim 150 \text{ Mpc}$. The comparison sample of SNe represents a literature compilation (see Figure 1 caption), with inferred mass loss rates spanning $\dot{M} \approx 10^{-7} - 10^{-2} M_\odot \text{ yr}^{-1}$ and a distribution peak near $\dot{M} \approx 10^{-5} M_\odot \text{ yr}^{-1}$ (see also Chevalier & Fransson 2006). We derive mass loss rates for SNe 2004cc, 2004dk, and 2004gq that overlap with the higher end of this SN Ibc distribution. In contrast, the engine-driven explosions considered here populate the low end of the mass loss rate distribution, $\dot{M} \approx (1-50) \times 10^{-7} M_\odot \text{ yr}^{-1}$.

A modest dispersion in the \dot{M} distribution may be expected due to variations in the shock partition fractions (ϵ_e, ϵ_B), how-

ever, these are unlikely to deviate strongly from the assumed values since they are reasonably constrained to be near equipartition with $\epsilon_e = \epsilon_B = [0.1, 0.33]$. Some dispersion in the \dot{M} distribution is also expected from an intrinsic spread in progenitor wind speeds; we emphasize that the radio observations only constrain the quantity, (\dot{M}/v_w) , and we have assumed a constant wind, $v_w = 10^3 \text{ km s}^{-1}$ for each SN. However, v_w is regulated by the progenitor escape speed and is not seen to vary by more than a factor of a few in the set of well-studied Galactic WRs (see §5). Therefore, the factor of 10^5 spread in the inferred mass loss rates of SN Ibc progenitors points an intrinsically broad dispersion⁷.

In comparison to other supernova sub-types, the mass loss rates for these SN Ibc progenitors are lower than those inferred for most Type IIn SNe, revealing intense progenitor mass loss episodes with $\dot{M} \approx 0.01 - 1 M_\odot \text{ yr}^{-1}$ and wind velocities of $v_w \approx 300 \text{ km s}^{-1}$ in the decades leading up to explosion (Smith 2008; Kiewe *et al.* 2012). The local CSM densities of SNe IIn are so high that the radio emission typically becomes optically-thin only years after the explosion in the cm-band such that the early radio signal is suppressed below detectable limits (e.g., SN 1988Z; Williams *et al.* 2002).

5. THE NATURE OF CSM DENSITY MODULATIONS

While it is generally understood that the massive progenitor stars of SNe Ibc (including relativistic SNe) lose their envelopes prior to explosion, the mechanism(s) by which the material is removed and the relevant timescale(s) remains debated (Smith *et al.* 2011). Here we review the possible causes of circumstellar density modulations in core-collapse SNe.

Isolated Wolf-Rayet stars, the favored progenitors of SNe Ibc, are seen to lose mass at a typical rate of $\dot{M} \approx (0.5 - 2) \times 10^{-5} M_\odot \text{ yr}^{-1}$ (including Galactic WN, WC, and WO subtypes; Cappa, Goss & van der Hucht 2004; Crowther 2007) through line-driven winds traveling at $v_w \approx (0.7 - 2.5) \times 10^3 \text{ km s}^{-1}$, propelled by radiation pressure and momentum coupling (Castor, Abbott & Klein 1975; Conti 1978). These winds shape the immediate circumstellar environment on sub-parsec scales. The strength of such line-driven winds scales almost linearly with metallicity ($\dot{M} \propto Z^{0.8}$; Vink & de Koter 2005), and an upper limit on this process is set by saturation of the metal lines at $\dot{M} \approx 10^{-4} M_\odot \text{ yr}^{-1}$. Small-scale clumping within the winds due to turbulence can produce moderate density modulations (factor of 2–4; see Moffat 2008). At similar circumstellar radii, modest density modulations may be present due to subtle variations in the stellar wind velocity. The collision of winds in a tight binary systems can also give rise to CSM density modulations in the immediate vicinity of the progenitor.

At larger circumstellar radii (a few parsec) an abrupt density jump is likely produced by a wind termination shock between the fast Wolf-Rayet wind and the slower red supergiant (RSG) wind (Garcia-Segura, Langer & Mac Low 1996). Numerical simulations indicate that the structure of the wind-termination shock is shell-like, and that the interaction of the SN shockwave with this density feature gives rise to a strong radio and X-ray signal, accompanied by hydrogen recombination lines in the optical band (e.g., Dwarkadas, Dewey & Bauer 2010).

Massive circumstellar shells are also produced in binary pro-

genitor systems where a common envelope is ejected by the motion of a companion star (Podsiadlowski, Joss & Hsu 1992). The envelope material moves more slowly ($v_w \approx 10 \text{ km s}^{-1}$) than the Wolf-Rayet wind and so becomes accelerated and compressed into a thin dense shell. The interaction of the shockwave with the common envelope shell produces an abrupt increase in the synchrotron emission and Balmer series recombination lines visible in optical spectra. Late-time radio and optical observations of SN 2001em revealed these characteristics (Soderberg, Gal-Yam & Kulkarni 2004; Stockdale *et al.* 2005), motivating Chugai & Chevalier (2006) to suggest that a common envelope was lost at a rate of $(2-10) \times 10^{-3} M_\odot \text{ yr}^{-1}$ and located at $r \approx 7 \times 10^{16} \text{ cm}$ at the time of the explosion.

Large density modulations may also be fueled by violent stellar outbursts such as those observed from Luminous Blue Variable stars (LBVs; Humphreys & Davidson 1994). LBVs are thought to represent a short-lived phase in the evolution of some supergiants, and immediately precede the development of classic WR features (Crowther 2007). Along this line, LBVs and WRs both show evidence for strong stellar winds and H-poor envelopes. LBVs give rise to giant mass loss ejections exceeding the saturation limit associated with line-driven winds and are therefore attributed to metallicity-independent continuum-driven winds and/or hydrodynamic eruptions (Smith & Owocki 2006). The outbursts result in dense and massive circumstellar shells that expand into a strong (and quasi-steady) wind. Multi-wavelength emission is observed from the resulting nebulae surrounding local LBVs on radial scales of $r \lesssim 1 \text{ pc}$ (e.g., Umana *et al.* 2010).

The long-lived and luminous multi-wavelength emission from Type IIn SNe is commonly attributed to the abrupt interaction of the shockwave with LBV-like mass ejections in the decades leading up to the explosion (e.g., Chugai *et al.* 2004). A recent (and extreme) example is the Type IIn SN 2006gy, for which a progenitor mass loss rate of $\dot{M} \approx 0.5 M_\odot \text{ yr}^{-1}$ has been inferred (Ofek *et al.* 2007; Smith *et al.* 2007; see van Marle *et al.* 2010 for a review). An intriguing aspect of the SN IIn mass loss histories is the synchronization required between the violent ejection episodes and the ultimate explosion (see Smith 2008 for a discussion). An LBV-like eruption seen from the Type Ib SN 2006jc progenitor star two years prior to explosion similarly indicates a synchronization, and in turn, a direct link between SN Ibc and IIn progenitors (Foley *et al.* 2007; Pastorello *et al.* 2007). At longer wavelengths, a link was also suggested by attributing the episodic radio variability observed for Type Ib/Ib SNe 2001ig and 2003bg to S-Doradus pulsations of the progenitor star (Kotak & Vink 2006, but see Soderberg *et al.* 2006a and Chevalier & Soderberg 2010 for a different interpretation).

5.1. SNe 2004cc, 2004dk, 2004gq

We consider the observed multi-wavelength properties for SNe 2004cc, 2004dk, and 2004gq in light of the various causes of circumstellar density modulations discussed above. As discussed in §4, the late-time radio data for these three SNe imply mass loss rates spanning $\dot{M} \approx (2-7) \times 10^{-5} M_\odot \text{ yr}^{-1}$ at circumstellar radii of $r \approx (1-50) \times 10^{16} \text{ cm}$. Their late-time radio variability implies circumstellar density modulations by a fac-

⁷We note that the subset of rare, radio luminous SNe are likely over-represented in this literature compilation since they are preferentially detected (e.g., SN 2003L; Soderberg *et al.* 2005; Chevalier & Fransson 2006). A distance-limited study of radio SN luminosities, and in turn, progenitor mass loss rates is required to determine the intrinsic dispersion in \dot{M} . This is the focus of a separate paper.

tor of $\sim 3-6$. Moreover, early optical photometry and late-time (nebular) spectroscopy are consistent with observations of typical SNe Ibc and do not reveal any evidence for unusually strong circumstellar interaction (e.g., H recombination lines; §2).

The intermediate-level density modulation factors and ordinary optical properties observed for these SNe indicate that it is unlikely that their shockwaves are interacting with a H-rich common envelope. Attributing the abrupt density modulations to a clumpy wind would imply that the clumps are exceedingly large (comparable to the size of the expanding shockwave) in order to produce an observable upward shift in the self-absorption frequency. This is inconsistent with the basic picture for small-scale, turbulence-driven WR wind clumps (e.g. Moffat 2008). Interaction with the wind termination shock should occur at significantly larger radii (several pc) so we find this scenario unlikely. However, it is possible to reduce the radius of the termination shock if these SNe are embedded in highly pressurized environments (Chevalier, Li & Fransson 2004) or if their progenitors were rapidly rotating prior to explosion (Cantiello *et al.* 2007).

In comparison to mass loss rates measured for Galactic Wolf-Rayet stars, the inferred circumstellar densities inferred for these three SNe are at the high end of the distribution (Figure 8). They show overlap with the mass loss rates inferred for radio luminous SNe 2003L and 2003bg on similar radial scales ($\dot{M} \approx 1-3 \times 10^{-4} M_{\odot} \text{ yr}^{-1}$; Chevalier & Fransson 2006), which are roughly consistent with the saturation limit for line-driven winds.

This, together with the abruptness of the mass loss variations and their apparent synchronization with respect to the explosion date, resembles the properties of SNe IIn. Their unusual mass loss properties may indicate some contribution from metallicity-independent envelope-stripping mechanisms (e.g., continuum-driven winds and/or hydrodynamic eruptions). While the density enhancements inferred here are not as extreme as those seen for Galactic LBVs or inferred for SN IIn progenitors, their abrupt nature is reminiscent.

5.2. A Metallicity Dependence?

A key question raised by these observations is whether the circumstellar environments inferred for some SNe are shaped by metallicity-dependent line-driven winds or “LBV-like” metallicity-independent mass loss mechanisms. While it is not possible to measure the metallicity of the progenitor star post-explosion, the metallicity of the explosion site on a sub-kpc scale may serve as a reasonable proxy for that of the short-lived progenitor system. A comparison between the explosion site metallicities and the radio-derived mass loss rates tests the metallicity-dependence of the envelope-stripping mechanism.

As a rough estimate of the explosion site metallicity, we adopt the absolute B -band magnitudes for the three host galaxies (Table 1) and the luminosity-metallicity relation of Tremonti *et al.* (2004). We find host galaxy metallicities of $[12+\log(\text{O/H})] \approx 8.9, 8.8$, and 9.0 for SNe 2004cc, 2004dk, and 2004gq, respectively. These estimates are somewhat higher than the solar metallicity, $[12+\log(\text{O/H})] \approx 8.69$ (Allende Prieto, Lambert & Asplund 2001). However, these values are *global* metallicity estimates, and there is evidence that the explosion site metallicities of SNe Ibc can be significantly differ-

ent than those estimated globally due to metallicity gradients within the host galaxy (see Anderson *et al.* 2010; Modjaz *et al.* 2011 for a discussion). Along this line, Anderson *et al.* (2010) recently reported an explosion site metallicity for SN 2004gq of $[12+\log(\text{O/H})] \approx 8.8$, lower than that estimated globally for the host galaxy⁸. Explosion site metallicities are currently unavailable for SN 2004cc and SN 2004dk; however, Modjaz *et al.* (2011) estimate that the offset between global and sub-kpc metallicities for SNe Ibc is typically of order ± 0.2 dex. We conclude that the explosion sites metallicities for these three SNe are likely typical, probably not far from the Solar value and consistent with the range of metallicities at which line-driven winds operate efficiently.

Finally we note that the current range of explosion site metallicities spans just 0.5 dex for ordinary SNe Ibc and engine-driven explosions (Modjaz *et al.* 2011). However, the dispersion in radio-derived mass loss rates spans several orders of magnitude, significantly broader than expected if the $\dot{M}-Z$ relation is roughly linear. This preliminary comparison suggests that metallicity-dependent mass loss processes (e.g., line driven-winds) are not the only mechanism by which the progenitor envelope is removed in SNe Ibc and/or engine-driven explosions.

6. CONCLUSIONS

We present extensive radio observations and detailed modeling for the three nearby Type Ibc SNe 2004cc, 2004dk, and 2004gq. We show that the physical properties of their shockwaves are typical of other SNe Ibc while their circumstellar environments are characterized by unusually strong density modulations. We conclude with the following points:

- The radio spectra for all three SNe are well described by a self-absorbed synchrotron spectrum with a relativistic e^- population characterized by $\gamma_m \sim 1-2$ and $p \approx 3$.
- Detailed modeling of the early radio data shows them to be consistent with free-expansion model in which a non-relativistic shock interacts with a stellar wind environment. We extract shockwave velocities of $v \sim 0.1-0.25c$ and energies of $E \approx (2-10) \times 10^{47} \text{ erg}$ at $\Delta t \approx 10 \text{ days}$.
- Each SN is characterized by a late-time radio re-brightening or fading which we attribute to abrupt and significant (factor of $\sim 3-6$) density modulations at circumstellar radii of, $r \approx (1-50) \times 10^{16} \text{ cm}$. The inferred mass loss rates rates lie at the high end of the \dot{M} -distribution measured for Galactic WRs
- If we attribute the density modulations to variations in the progenitor mass loss rates then they approach the saturation limit for line-driven winds. If the density modulations are instead due to the collision with a wind termination shock, the SNe must reside in highly pressurized environments *or* be rapidly rotating prior to explosion in order to squeeze the termination shock to small circumstellar radii.
- The possible synchronization of the mass loss variations with the SN explosion is reminiscent of SN IIn progenitors.

⁸We note, however, that the explosion site metallicity was estimated using the emission line metallicity diagnostic of Pettini & Pagel (2004) which prevents a direct comparison of the two Z -estimates.

- A comparison of the radio-derived \dot{M} estimates and explosion site metallicities for stripped envelope SNe could shed light on the primary mass loss mechanism(s).

Finally, we note that that the strong flux density variations reported here are unlikely to be ubiquitous since they are recoverable by radio campaigns designed to search for off-axis GRB jets associated with SNe Ibc on timescales of months to years after explosion (Perna & Loeb 1998; Paczynski 2001). Such radio searches have uncovered strong late-time variability in less than $\sim 10\%$ of all SNe Ibc (Berger *et al.* 2003a; Soderberg *et al.* 2006c). Future radio efforts will shed light on the variability of radio SNe over various time baselines and therefore able

to probe density modulations at a wide-range of circumstellar radii. In particular, the improved sensitivity of the Expanded Very Large Array (Perley *et al.* 2009) will enable detailed monitoring of radio SNe to longer timescales, enabling the search for variable progenitor mass loss histories at larger circumstellar radii, possibly associated with earlier pre-explosion epochs.

We thank Norbert Langer, Stan Owocki, Nathan Smith, Vikram Dwarkadas, and Shri Kulkarni for helpful discussions. S.W. and A.M.S. acknowledge support by the National Science Foundation Research Experiences for Undergraduates (REU) and Department of Defense Awards to Stimulate and Support Undergraduate Research Experiences (ASSURE) programs under Grant no. 0754568 and by the Smithsonian Institution.

References

Allende Prieto, C., Lambert, D. L., and Asplund, M. 2001, *ApJ*, 556, L63.

Anderson, J. P., Covarrubias, R. A., James, P. A., Hamuy, M., and Habergham, S. M. 2010, *MNRAS*, 407, 2660.

Arcavi, I. *et al.* 2010, *ApJ*, 721, 777.

Ball, L., Campbell-Wilson, D., Crawford, D. F. and Turtle, A. J. 1995, *ApJ*, 453, 864.

Bauer, F. *et al.* 2008, *ApJ*, 688, 1210.

Begelman, M. C. and Sarazin, C. L. 1986, *ApJ*, 302, L59.

Berger, E., Kulkarni, S. R., and Chevalier, R. A. 2002, *ApJ*, 577, L5.

Berger, E., Kulkarni, S. R., Frail, D. A., and Soderberg, A. M. 2003a, *ApJ*, 599, 408.

Berger, E. *et al.* 2003b, *Nature*, 426, 154.

Bietenholz, M. F. *et al.* 2010, *ApJ*, 725, 4.

Cantiello, M., Yoon, S.-C., Langer, N., and Livio, M. 2007, *A&A*, 465, L29.

Cappa, C., Goss, W. M., and van der Hucht, K. A. 2004, *AJ*, 127, 2885.

Cappellaro, E., Evans, R., and Turatto, M. 1999, *A&A*, 351, 459.

Castor, J. I., Abbott, D. C., and Klein, R. I. 1975, *ApJ*, 195, 157.

Chevalier, R. A. 1992, *ApJ*, 258, 790.

Chevalier, R. A. 1998, *ApJ*, 499, 810.

Chevalier, R. A. and Dwarkadas, V. V. 1995, *ApJ*, 452, L45+.

Chevalier, R. A. and Fransson, C. 2006, *ApJ*, 651, 381.

Chevalier, R. A., Li, Z.-Y., and Fransson, C. 2004, *ApJ*, 606, 369.

Chevalier, R. A. and Soderberg, A. M. 2010, *ApJ*, 711, L40.

Chugai, N. N. *et al.* 2004, *MNRAS*, 352, 1213.

Chugai, N. N. and Chevalier, R. A. 2006, *ApJ*, 641, 1051.

Clocchiatti, A., Wheeler, J. C., Benetti, S. & Frueh, M. 1986, *ApJ*, 459, 547.

Conti, P. S. 1978, *ARA&A*, 16, 371.

Crowther, P. A. 2007, *ARA&A*, 45, 177.

Drout, M., Soderberg, A. M., Gal-Yam, A., and Cenko, S. B. 2011, *ApJ*, 741, 97.

Dwarkadas, V. V., Dewey, D., and Bauer, F. 2010, *MNRAS*, 965.

Elias, J. H., Matthews, K., Neugebauer, G. & Persson, S. E. 1985, *ApJ*, 296, 379.

Filippenko, A. V. & Sargent, W. L. W. *Nature*, 316, 407.

Filippenko, A. V. 1997, *ARA&A*, 35, 309.

Filippenko, A. V., Ganeshalingam, M., Serduke, F. J. D., and Hoffman, J. L. 2004, *IAU Circ.*, 8404, 1.

Foley, R. J., Wong, D. S., Moore, M. & Filippenko, A. V. 2004, *IAU Circ.*, 8353, 3.

Foley, R. J., Smith, N., Ganeshalingam, M., Li, W., Chornock, R., and Filippenko, A. V. 2007, *ApJ*, 657, L105.

Frail, D. A., Soderberg, A. M., Kulkarni, S. R., Berger, E., Yost, S., Fox, D. W., and Harrison, F. A. 2005, *ApJ*, 619, 994.

Fransson, C. and Björnsson, C. 1998, *ApJ*, 509, 861.

Fryer, C. L. *et al.* 2007, *PASP*, 119, 1211.

Garcia-Segura, G., Langer, N., and Mac Low, M. 1996, *A&A*, 316, 133.

Graham, J. and Li, W. 2004, *IAU Circ.*, 8377, 2.

Hamuy, M. *et al.* 2002, *AJ*, 124, 417.

Humphreys, R. M. and Davidson, K. 1994, *PASP*, 106, 1025.

Kellermann, K. and Pauliny-Toth, I. 1968, *ARA&A*, 6, 417.

Kiewe, M. *et al.* 2012, *ApJ*, 744, 10.

Kotak, R. and Vink, J. S. 2006, *A&A*, 460, L5.

Krauss, M. *et al.* 2012, *ApJ*, (submitted).

Kulkarni, S. R. *et al.* 1998, *Nature*, 395, 663.

Levesque, E. M., Berger, E., Kewley, L. J. & Bagley, M. M. 2010, *ApJ*, 139, 694.

Li, W. *et al.* 2000, *AIPC*, 522, 103.

Li, W. *et al.* 2011, *MNRAS*, 412, 1441.

Maeda, K. *et al.* 2008, *Science*, 319, 1220.

MacFadyen, A. I., Woosley, S. E. & Heger, A. 2001, *ApJ*, 550, 410.

Matheson, T., Challis, P., Kirshner, R., and Penev, K. 2004, *IAU Circ.*, 8353, 2.

Matheson, T., Filippenko, A. V., Li, W., Leonard, D. C., and Shields, J. C. 2001, *AJ*, 121, 1648.

Matzner, C. D. and McKee, C. F. 1999, *ApJ*, 510, 379.

Mazzali, P. A. *et al.* 2003, *ApJ*, 599, L95.

Modjaz, M., *et al.* 2011, *ApJ*, 731, 4.

Modjaz, M. and Falco, E. 2005, *IAU Circ.*, 8461, 3.

Modjaz, M. *et al.* 2008, *AJ*, 135, 1136.

Moffat, A. F. J. 2008, in *Clumping in Hot-Star Winds*, ed. W.-R. Hamann, A. Feldmeier, & L. M. Oskinova, 17.

Monard, L. A. G. and Li, W. 2004, *IAU Circ.*, 8350, 2.

Ofek, E. O. *et al.* 2007, *ApJ*, 659, L13.

Paczynski, B. 2001, *Acta Astronomica*, 51, 1.

Pastorello, A. *et al.* 2007, *Nature*, 447, 829.

Perley, R. *et al.* 2009, *IEEE Proceedings*, 97, 1448.

Perna, R. and Loeb, A. 1998, *ApJ*, 509, L85.

Pettini, M. and Pagel, B. E. J. 2004, *MNRAS*, 348, L59.

Podsiadlowski, P., Joss, P. C., and Hsu, J. J. L. 1992, *ApJ*, 391, 246.

Podsiadlowski, P., *et al.* 2004, *ApJ*, 607, L17.

Pooley, D. 2007, in *Supernova 1987A: 20 Years After: Supernovae and Gamma-Ray Bursters*, ed. S. Immler, K. Weiler, & R. McCray, volume 937 of *American Institute of Physics Conference Series*, 381.

Pugh, H., Li, W., Manzini, F., and Behrend, R. 2004, *IAU Circ.*, 8452, 2.

Roming, P. W. A. *et al.* 2009, *ApJ*, 704, L118.

Rybicki, G. B. and Lightman, A. P. 1979, *Radiative processes in astrophysics*,).

Ryder, S. D., Sadler, E. M., Subrahmanyan, R., Weiler, K. W., Panagia, N., and Stockdale, C. 2004, *MNRAS*, 349, 1093.

Shklovskii, I. S. *Astronomicheskii Zhurnal*, 37, 256.

Smartt, S. J. 2009, *ARA&A*, 47, 63.

Smith, N. 2008, in *IAU Symposium*, ed. F. Bresolin, P. A. Crowther, & J. Puls, volume 250 of *IAU Symposium*, 193.

Smith, N., Li, W., Filippenko, A. V., and Chornock, R. 2011, *MNRAS*, 412, 1522.

Smith, N. *et al.* 2007, *ApJ*, 666, 1116.

Smith, N. and Owocki, S. P. 2006, *ApJ*, 645, L45.

Soderberg, A. M. 2007, in *Supernova 1987A: 20 Years After: Supernovae and Gamma-Ray Bursters*, ed. S. Immler, K. Weiler, & R. McCray, volume 937 of *American Institute of Physics Conference Series*, 492.

Soderberg, A. M. 2009, *The Astronomer's Telegram*, 2066, 1.

Soderberg, A. M. *et al.* 2008, *Nature*, 453, 469.

Soderberg, A. M., Brunthaler, A., Nakar, E., Chevalier, R. A., and Bietenholz, M. F. 2010b, *ApJ*, 725, 922.

Soderberg, A. M. *et al.* 2010a, *Nature*, 463, 513.

Soderberg, A. M., Chevalier, R. A., Kulkarni, S. R., and Frail, D. A. 2006a, *ApJ*, 651, 1005.

Soderberg, A. M., Gal-Yam, A., and Kulkarni, S. R. 2004, *GRB Coordinates Network*, 2586, 1.

Soderberg, A. M., Kulkarni, S. R., Berger, E., Chevalier, R. A., Frail, D. A., Fox, D. B., and Walker, R. C. 2005, *ApJ*, 621, 908.

Soderberg, A. M. *et al.* 2006b, *Nature*, 442, 1014.

Soderberg, A. M., Nakar, E., Berger, E., and Kulkarni, S. R. 2006c, *ApJ*, 638, 930.

Sramek, R. A., Panagia, N., and Weiler, K. W. 1984, *ApJ*, 285, L59.

Stockdale, C. J. *et al.* 2009, *Central Bureau Electronic Telegrams*, 1714, 1.

Stockdale, C. J. *et al.* 2005, *IAU Circ.*, 8472, 4.

Tremonti, C. A. *et al.* 2004, *ApJ*, 613, 898.

Umana, G., Buemi, C. S., Trigilio, C., Leto, P., Hora, J. L., and Fazio, G. 2010, *ArXiv e-prints*.

Uomoto, A. & Kirshner, R. P. 1985, *A&A*, 149, L7.

van Dyk, S. D., Sramek, R. A., Weiler, K. W., and Panagia, N. 1993, *ApJ*, 409, 162.

van Marle, A. J., Smith, N., Owocki, S. P., and van Veelen, B. 2010, *MNRAS*, 407, 2305.

Vink, J. S. and de Koter, A. 2005, *A&A*, 442, 587.

Weiler, K. 2006, in *KITP Conference: Supernova and Gamma-Ray Burst Remnants*.

Weiler, K. W., van Dyk, S. D., Discenna, J. L., Panagia, N., and Sramek, R. A. 1991, ApJ, 380, 161.

Weiler, K. W., Williams, C. L., Panagia, N., Stockdale, C. J., Kelley, M. T., Sramek, R. A., Van Dyk, S. D., and Marcaide, J. M. 2007, ApJ, 671, 1959.

Wheeler, J. C. and Levreault, R. 1985, ApJ, 294, L17.

Williams, C. L., Panagia, N., Van Dyk, S. D., Lacey, C. K., Weiler, K. W., and Sramek, R. A. 2002, ApJ, 581, 396.

Woosley, S. E., Langer, N., and Weaver, T. A. 1995, ApJ, 448, 315.

Woosley, S. E., Heger, A. & Weaver, T. A. 2002, *Reviews of Modern Physics*, 74, 1015.

Yoon, S.-C., Woosley, S. E. & Langer, N. 2010, ApJ, 725, 940.

Zanardo, G. *et al.* 2010, ApJ, 710, 1515.

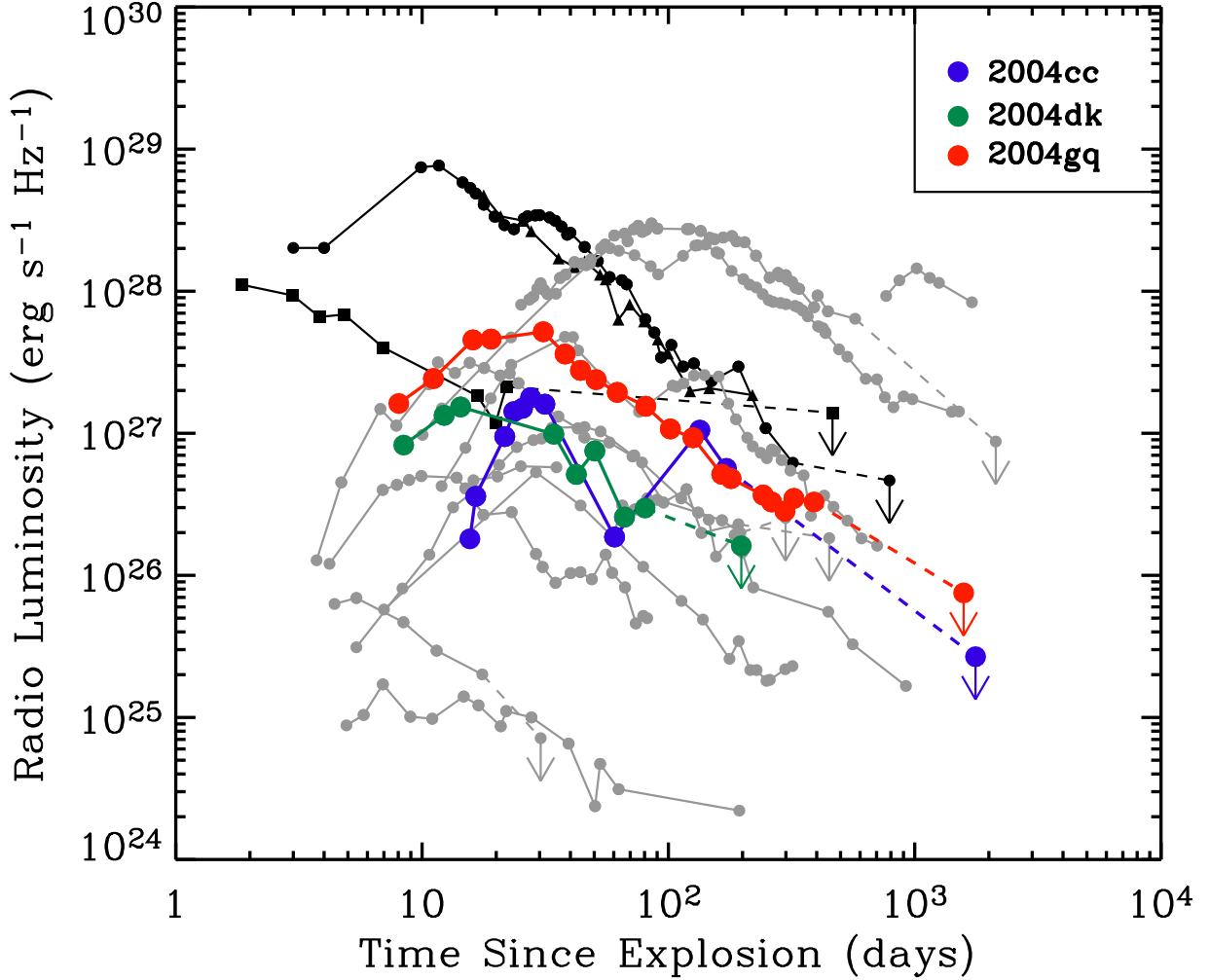


FIG. 1.— Radio light curves for 2004cc (blue), 2004dk (green), 2004gq (red), are compared with other Type Ibc supernovae, including SNe 1983N (Sramek, Panagia & Weiler 1984), 1990B (van Dyk *et al.* 1993), 1994I (Weiler 2006), 2001ig (Ryder *et al.* 2004), 2002ap (Berger, Kulkarni & Chevalier 2002), 2003L (Soderberg *et al.* 2005), 2003bg (Soderberg *et al.* 2006a), 2007gr (Soderberg *et al.* 2010b), 2008D (Soderberg *et al.* 2008), 2008ax (Roming *et al.* 2009), and 2011dh (Krauss *et al.* 2012) all shown in grey. The radio afterglows of nearby engine-driven explosions within a similar volume are shown in black, including GRB-SN 1998bw (circles; Kulkarni *et al.* 1998), XRF-SN 2006aj (squares; Soderberg *et al.* 2006b), and SN 2009bb (triangles; Soderberg *et al.* 2010a). SNe 2004cc, 2004dk, and 2004gq are similar in radio luminosity to ordinary radio SNe and less luminous than engine-driven explosions on a similar timescale.

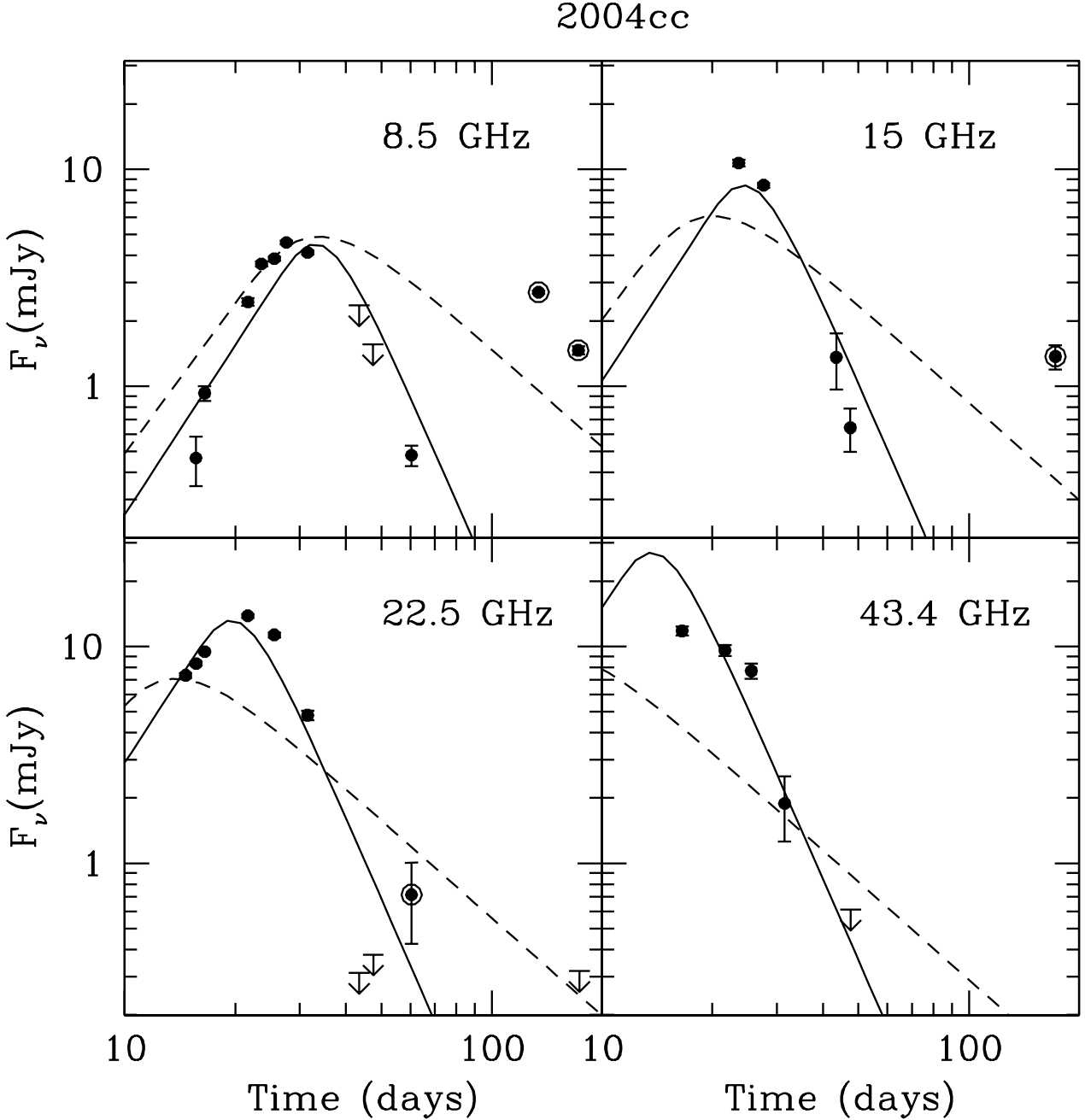


FIG. 2.— Radio observations of SN 2004cc are shown at various frequencies and compared to our dynamical models. Dashed lines represent the model parametrization assuming a density profile of $n_e \propto r^{-2}$. We find a significantly better fit (solid lines) associated with a steeper density profile. Encircled data points indicate an unusual late-time re-brightening and were not included in the model fits.

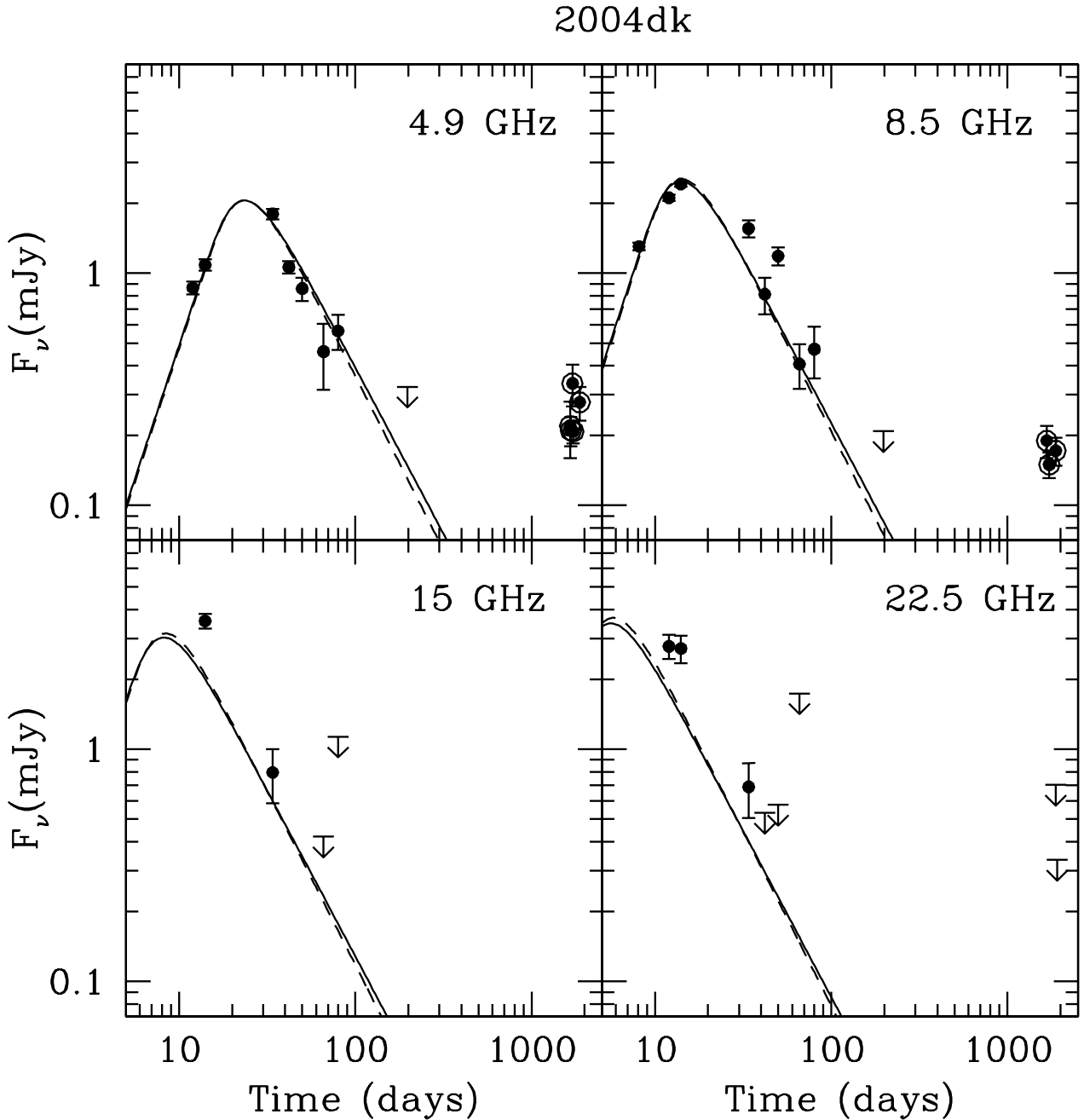


FIG. 3.— Radio observations of SN 2004dk are shown at various frequencies and compared to our dynamical models. The solid lines represent the best fit model parametrization, while the dashed lines represent a model in which the density profile is fixed as $n_e \propto r^{-2}$. Encircled data points at indicate an unusual late-time re-brightening and were not included in the model fits, shown in detail in Fig. 4.

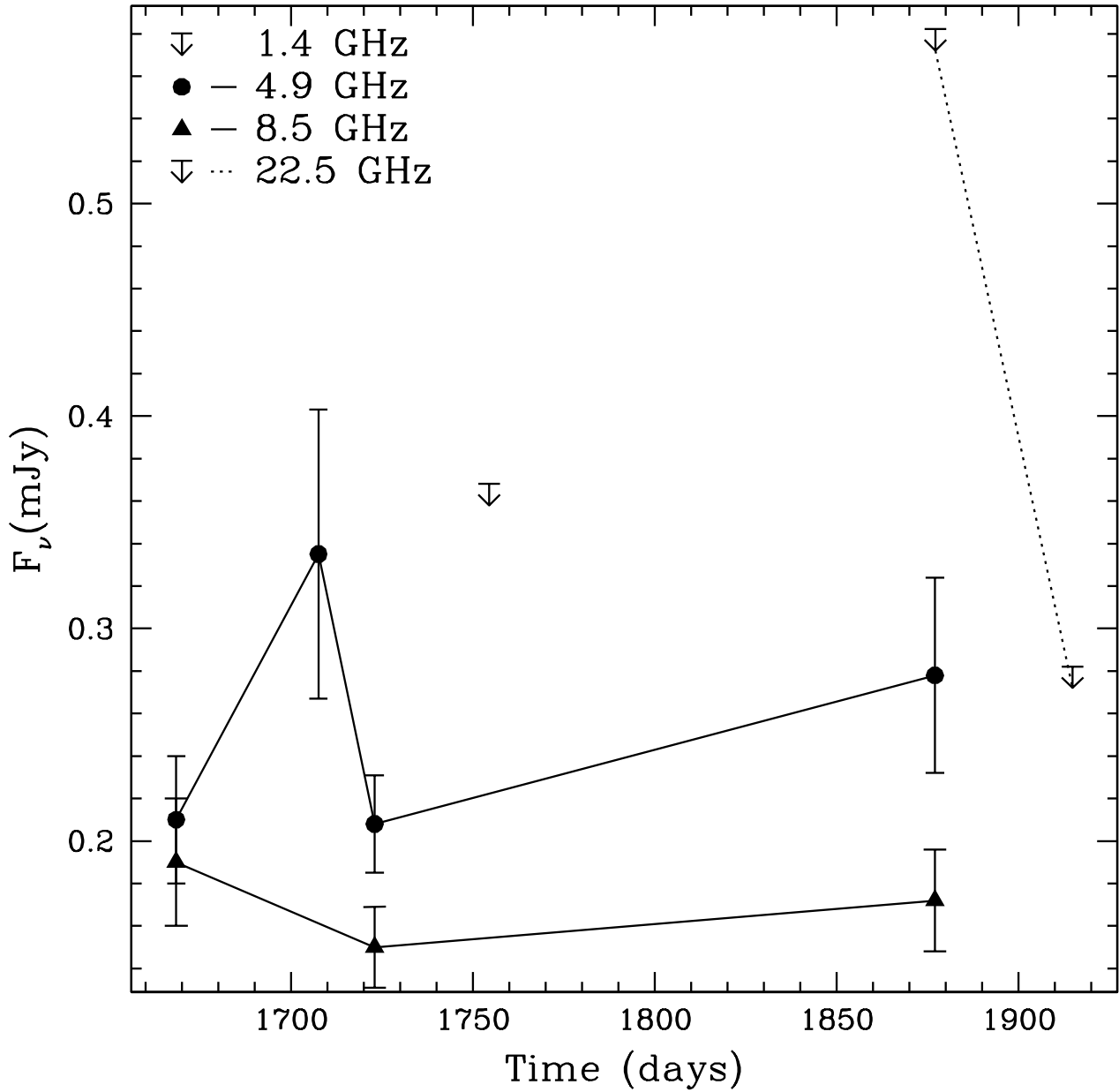


FIG. 4.— Radio observations of SN 2004dk at late time, during the rebrightening episode, are shown at several frequencies. The SN is optically thin throughout the rebrightening.

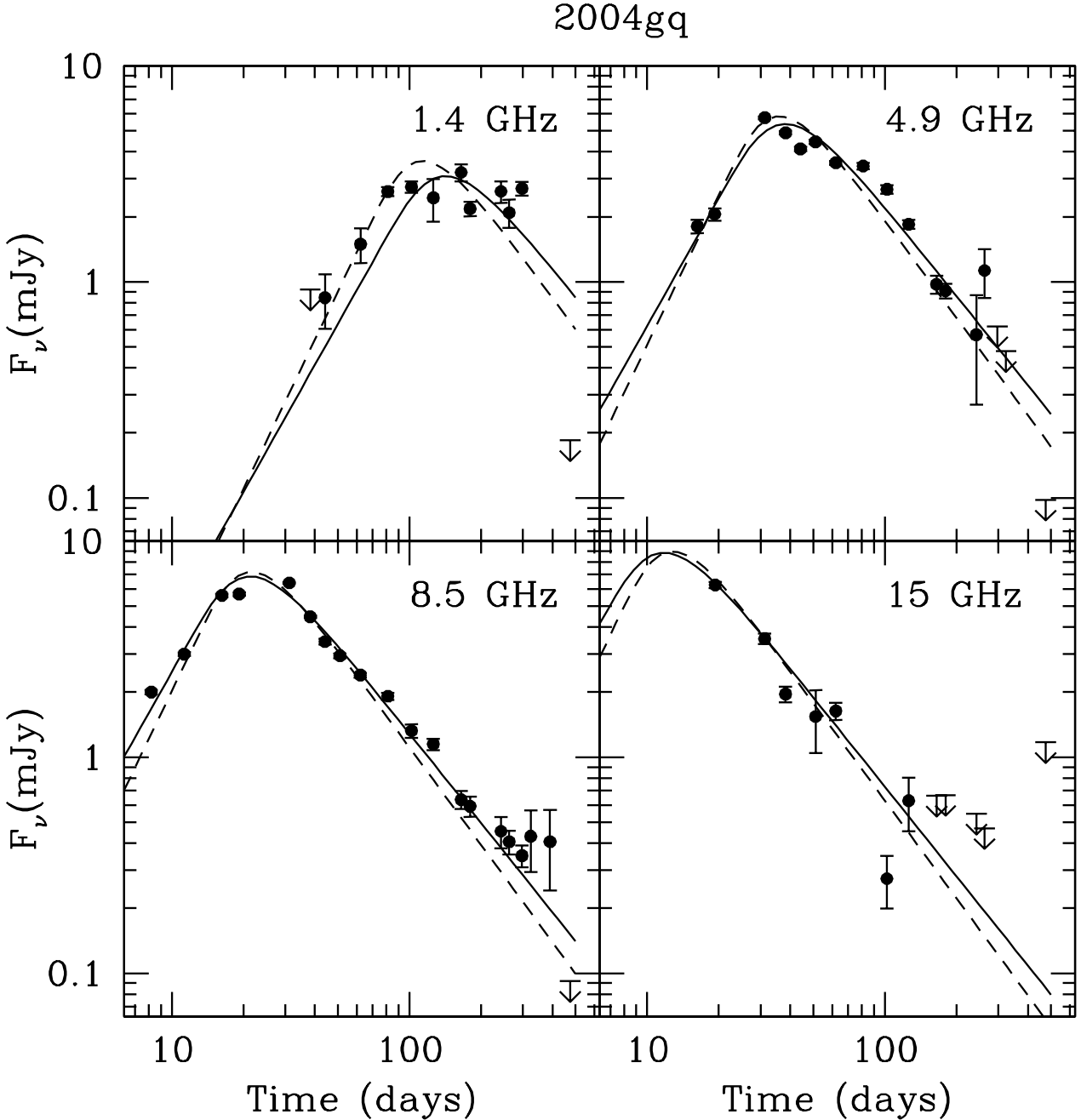


FIG. 5.— Radio observations of SN 2004dk are shown at various frequencies and compared to our dynamical models. The solid lines represent the best fit model parametrization, while the dashed lines represent a model parametrization in which the density profile is fixed to $n_e \propto r^{-2}$. The deep limits at late-time indicate an unusual steepening of the radio flux and were not included in the model fits.

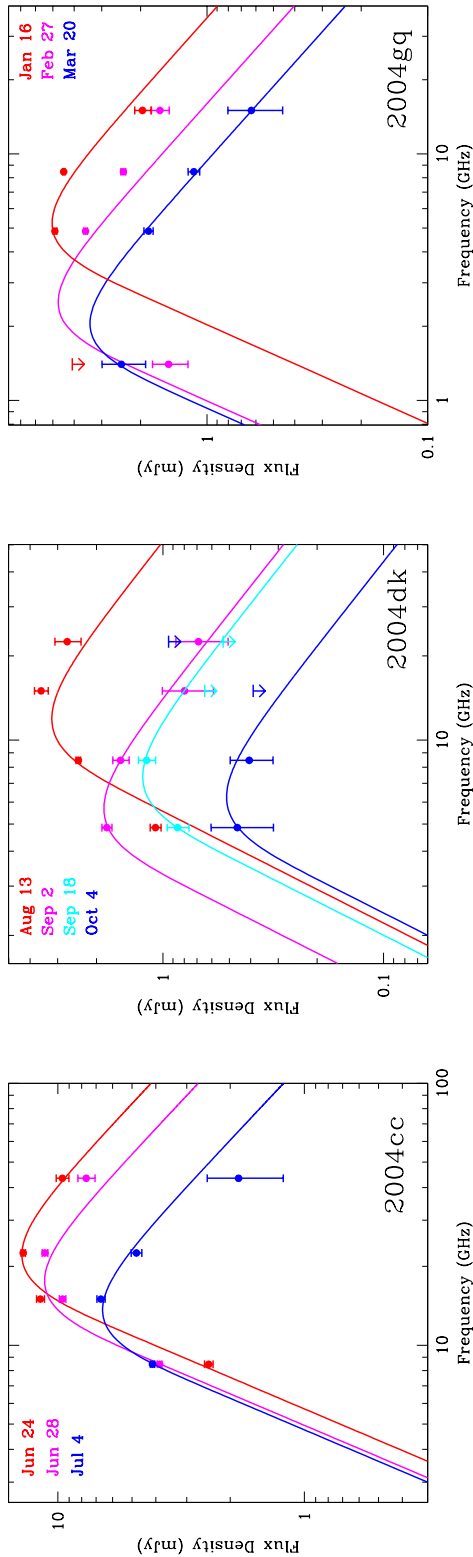


FIG. 6.— Multi-frequency radio observations of SNe 2004cc, 2004dk, and 2004gq are well described by an SSA spectrum with $F_\nu \propto \nu^{5/2}$ in the optically thick regime and $F_\nu \propto \nu^{-1}$ in the optically thin regime, associated with an electron index of $p \approx 3$.

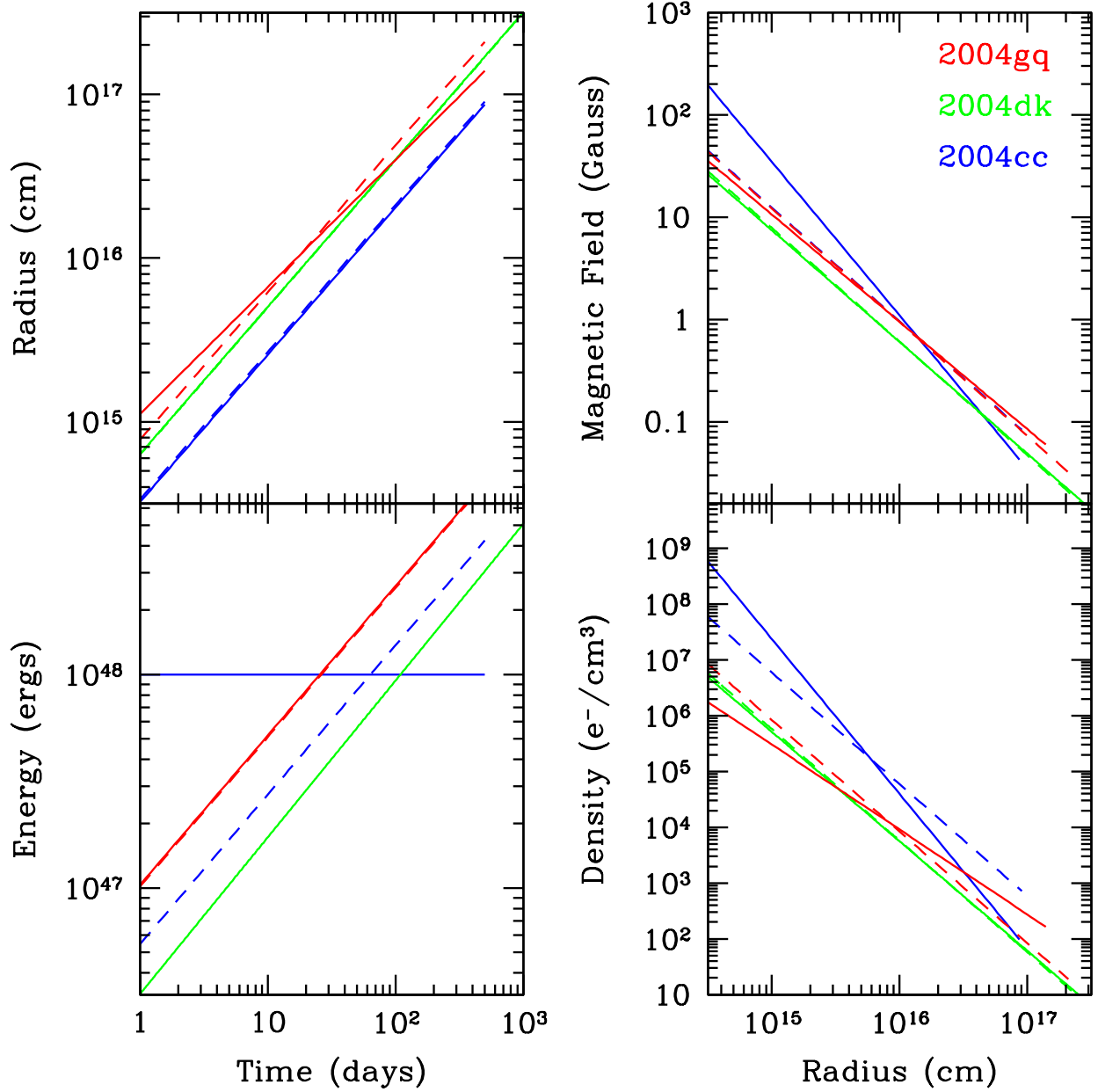


FIG. 7.— The derived temporal and radial properties of the shockwave and local environment are compared for SNe 2004cc (blue), 2004dk (green), and 2004gq (red). The solid lines represent the best-fit parametrization of our dynamical model while the dashed lines correspond to a parameterization with a CSM density profile fixed to $n \propto r^{-2}$.

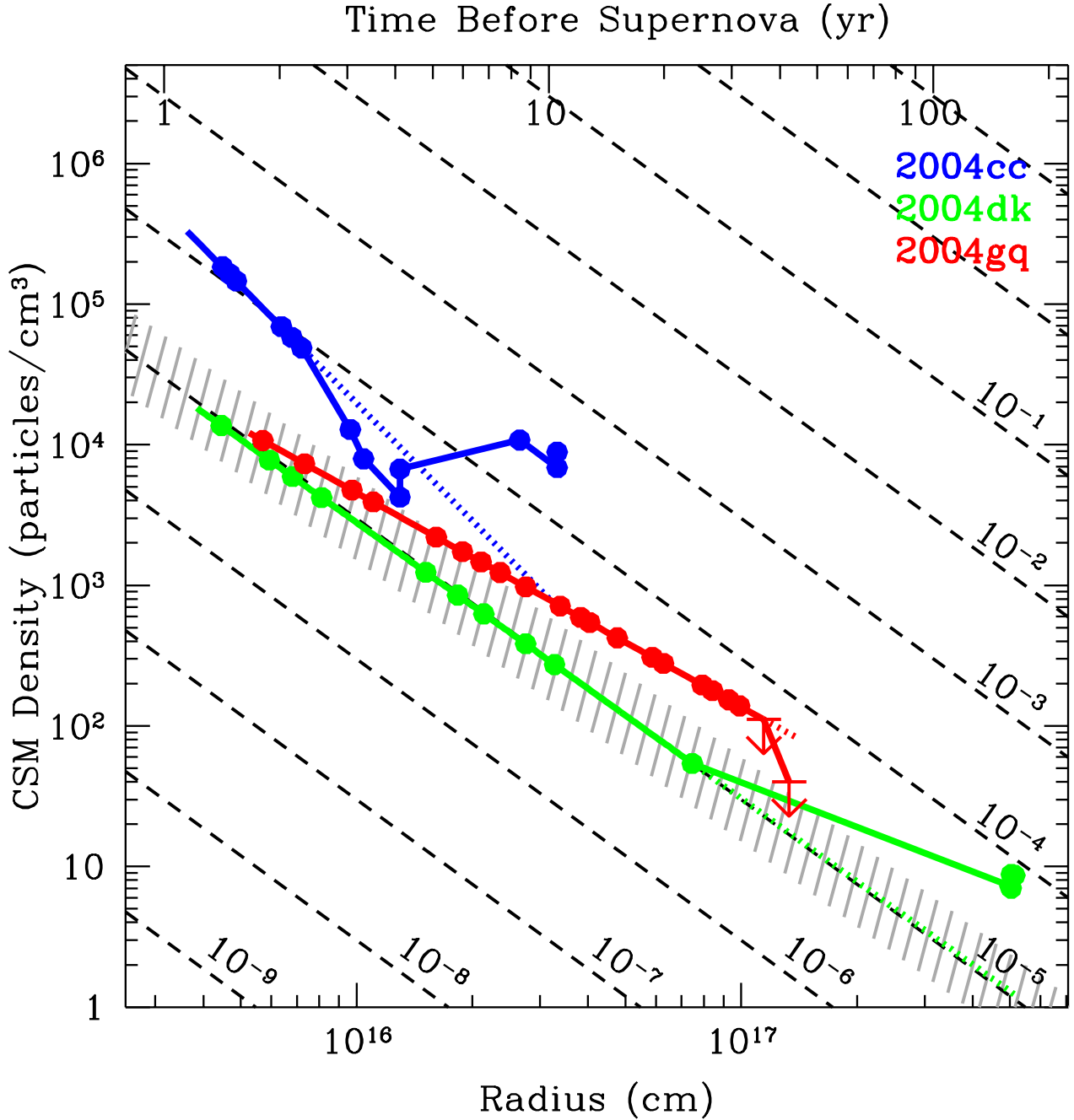


FIG. 8.— The density profile of shocked particles is shown as a function of circumstellar radius for SNe 2004cc (blue), 2004dk (green), and 2004gq (red). Modeling of the early data imply density values shown by the color dotted lines. The abrupt deviations from these fits at later epochs are associated with CSM density modulations. Radially averaged mass loss rates are shown for comparison (black dashed lines). The grey hatched region marks the observed range of mass loss rates for Galactic Wolf-Rayet stars. Assuming a wind velocity of 1000 km/s, these density modulations could be attributed to variable progenitor mass loss on a timescale of $\sim 10-100$ years before explosion (top axis).

TABLE 1
SN SAMPLE PROPERTIES

Name	Host Galaxy	Distance ¹ (Mpc)	Host Magnitude (M_B)	Disc. Date ² (UT)	Explosion Date (UT)	Type	$F_{p,8.5\text{ GHz}}$ (mJy)	$t_{p,8.5\text{ GHz}}$ (days)
2004cc	NGC 4568	18 ± 2	-19.6 ± 0.3	2004 Jun 10	2004 Jun 2	Ic	4.5	32
2004dk	NGC 6118	23 ± 2	-19.4 ± 0.3	2004 Aug 1	2004 Jul 30	Ib	2.5	14
2004gq	NGC 1832	26 ± 5	-20.1 ± 0.7	2004 Dec 11	2004 Dec 8	Ib	6.9	21

¹We adopt cosmology independent distances from NED-1D when available, otherwise we adopt the model-derived NED distances assuming $H_0 = 73 \text{ km s}^{-1} \text{ Mpc}^{-1}$, $\Omega_M = 0.27$, and $\Omega_\Lambda = 0.73$.

²We estimate the explosion date by the linear mean of the UT dates bridging the optical SN discovery and the most recent pre-discovery non-detection.

TABLE 2
OBSERVATIONS OF SN 2004CC

Date (UT)	$F_{\nu,8.5\text{ GHz}}$ (mJy)	$F_{\nu,15\text{ GHz}}$ (mJy)	$F_{\nu,22.5\text{ GHz}}$ (mJy)	$F_{\nu,43.4\text{ GHz}}$ (mJy)	VLA Config.
2004 Jun 17.2	7.35 ± 0.18	...	D
2004 Jun 18.1	0.47 ± 0.12	...	8.33 ± 0.16	...	D
2004 Jun 19.0	0.93 ± 0.07	...	9.44 ± 0.11	11.79 ± 0.55	D
2004 Jun 24.2	2.44 ± 0.10	...	13.83 ± 0.29	9.60 ± 0.57	D
2004 Jun 26.1	3.66 ± 0.10	10.69 ± 0.37	D
2004 Jun 28.1	3.87 ± 0.09	...	11.29 ± 0.30	7.70 ± 0.61	D
2004 Jun 30.1	4.60 ± 0.09	8.44 ± 0.21	D
2004 Jul 4.0	4.13 ± 0.08	...	4.81 ± 0.24	1.89 ± 0.63	D
2004 Jul 16.0	< 2.36	1.36 ± 0.40	< 0.31	...	D
2004 Jul 20.0	< 1.56	0.64 ± 0.15	< 0.38	< 0.61	D
2004 Aug 1.9	0.48 ± 0.05	...	0.72 ± 0.29	...	D
2004 Oct 14.6	2.71 ± 0.05	A
2004 Nov 21.6	1.46 ± 0.06	1.37 ± 0.18	< 0.21	...	A
2009 Feb 3.3	< 0.05	B

TABLE 3
OBSERVATIONS OF SN 2004DK

Date (UT)	$F_{\nu,4.9 \text{ GHz}}$ (mJy)	$F_{\nu,8.5 \text{ GHz}}$ (mJy)	$F_{\nu,15 \text{ GHz}}$ (mJy)	$F_{\nu,22.5 \text{ GHz}}$ (mJy)	VLA Config.
2004 Aug 7.1	...	1.30 ± 0.05	D
2004 Aug 11.0	0.87 ± 0.06	2.11 ± 0.06	...	2.78 ± 0.33	D
2004 Aug 13.0	1.09 ± 0.06	2.42 ± 0.06	3.57 ± 0.26	2.72 ± 0.37	D
2004 Aug 18.1 [†]	0.95 ± 0.07	1.76 ± 0.07	0.83 ± 0.23	1.75 ± 0.46	D
2004 Sep 2.0	1.80 ± 0.09	1.56 ± 0.13	0.79 ± 0.21	0.69 ± 0.18	D
2004 Sep 10.0	1.06 ± 0.07	0.81 ± 0.15	...	< 0.43	A
2004 Sep 18.0	0.86 ± 0.10	1.19 ± 0.11	...	< 0.47	A
2004 Oct 4.1	0.46 ± 0.15	0.41 ± 0.09	< 0.34	< 1.41	A
2004 Oct 17.8	0.56 ± 0.10	0.47 ± 0.12	< 0.92	...	A
2005 Feb 12.4	< 0.26	< 0.17	BnA
2009 Feb 12.6*	0.22 ± 0.06	B
2009 Feb 24.5*	0.21 ± 0.03	0.19 ± 0.03	B
2009 Apr 2.6	0.34 ± 0.07	< 0.08	B
2009 Apr 19.0 [‡]	0.21 ± 0.02	0.15 ± 0.02	C
2009 Sep 19.8	0.28 ± 0.05	0.17 ± 0.02	...	< 0.57	B
2009 Oct 26.8	< 0.27	D

[†]Poor weather on 2004 Aug 18.1.

^{*}Flux density values reported by Stockdale *et al.* (2009).

[‡]Observations also conducted at 1.4 GHz revealing a flux density of 0.18 ± 0.09 mJy.

TABLE 4
OBSERVATIONS OF SN 2004GQ

Date (UT)	$F_{\nu,1.4 \text{ GHz}}$ (mJy)	$F_{\nu,4.9 \text{ GHz}}$ (mJy)	$F_{\nu,8.5 \text{ GHz}}$ (mJy)	$F_{\nu,15 \text{ GHz}}$ (mJy)	VLA Config.
2004 Dec 16.2	2.00 ± 0.05	...	A
2004 Dec 19.3	3.00 ± 0.06	...	A
2004 Dec 24.3	...	1.81 ± 0.13	5.61 ± 0.10	...	A
2004 Dec 27.2	...	2.06 ± 0.14	5.68 ± 0.11	6.27 ± 0.22	A
2005 Jan 8.2	...	5.75 ± 0.09	6.40 ± 0.06	3.53 ± 0.20	A
2005 Jan 15.2	< 0.92	4.90 ± 0.10	4.47 ± 0.05	1.96 ± 0.17	A
2005 Jan 21.1	0.85 ± 0.24	4.12 ± 0.09	3.43 ± 0.10	...	BnA
2005 Jan 28.1	...	4.45 ± 0.10	2.95 ± 0.08	1.54 ± 0.50	BnA
2005 Feb 8.2	1.49 ± 0.27	3.56 ± 0.08	2.40 ± 0.06	1.64 ± 0.15	BnA
2005 Feb 27.1	2.62 ± 0.13	3.44 ± 0.12	1.91 ± 0.07	...	B
2005 Mar 13.0	2.45 ± 0.55	B
2005 Mar 20.0	2.75 ± 0.16	2.68 ± 0.12	1.33 ± 0.09	0.27 ± 0.08	B
2005 Apr 13.0	...	1.84 ± 0.09	1.15 ± 0.07	0.63 ± 0.18	B
2005 May 21.9	3.21 ± 0.29	0.97 ± 0.09	0.64 ± 0.06	< 0.66	B
2005 Jun 5.8	2.18 ± 0.17	0.91 ± 0.07	0.59 ± 0.06	< 0.67	B
2005 Aug 7.6	2.62 ± 0.30	0.57 ± 0.30	0.45 ± 0.07	< 0.55	C
2005 Aug 27.6	2.09 ± 0.31	1.13 ± 0.29	0.41 ± 0.05	< 0.47	C
2005 Oct 1.5	2.71 ± 0.20	< 0.62	0.35 ± 0.04	...	C
2005 Oct 27.4	...	< 0.48	0.43 ± 0.14	...	DnC
2006 Jan 2.3	0.41 ± 0.05	...	D
2006 Mar 26.9	< 0.10	< 0.09	< 0.14	< 1.17	A
2009 Apr 6.0	< 0.08	...	B

TABLE 5
MODEL PARAMETER FITS

	2004cc Best Fit	2004cc Fixed $n \propto r^{-2}$	2004dk Best Fit	2004dk Fixed $n \propto r^{-2}$	2004gq Best Fit	2004gq Fixed $n \propto r^{-2}$
$C_f (\times 10^{-52})$	5.0	7.7	31	30	39	32
$C_\tau (\times 10^{38})$	0.30	1.9×10^{-2}	6.2×10^{-4}	6.8×10^{-4}	2.4×10^{-3}	3.4×10^{-3}
α_R	0.9	0.9	0.9	0.9	0.8	0.9
α_B	-1.4	-1.0	-1.0	-1.0	-0.8	-1.0
s	2.8	2.0	2.0	2.0	1.5	2.0
R_0 (cm)	2.6×10^{15}	2.7×10^{15}	5.0×10^{15}	5.0×10^{15}	6.7×10^{15}	6.2×10^{15}
$\overline{v_0}$ (c)	0.10	0.10	0.20	0.19	0.26	0.24
B_0 (G)	8.4	4.2	1.3	1.3	1.5	1.6
$E_0 (\times 10^{47} \text{ erg})$	10	2.7	1.7	1.8	5.2	5.1
$n_{e,0} (\times 10^4 e^- / \text{cm}^3)$	170	83	2.2	2.3	1.7	2.2
$\gamma_{m,0}$	1	1	1.8	1.8	3.0	2.9
$\dot{M}_0 (\times 10^{-5} M_\odot \text{ yr}^{-1})$	13	6.5	0.60	0.63	0.83	0.92
Modulation Epoch	40,135	...	1708	...	474	...
Abruptness Factor	0.27, 1.2	...	7.7	...	0.21	...
Modulation Factor	< 2.5, 11	2.9	40	53	< 0.20	< 0.28

NOTE.—The subscript “0” denotes the parameter values at $\Delta t \approx 10$ days since explosion.